Running Title

MD simulations of glucocorticoid receptor mutants

Title

Molecular Dynamics Studies of a Molecular Switch in the Glucocorticoid Receptor.

Thomas Stockner[†], Heinz Sterk[†], Robert Kaptein[‡], Alexandre M. J. J. Bonvin[‡*]

[†] Karl Franzens Universität Graz, Department of NMR Spectroscopy, Heinrichstrasse 28, 8010 Graz, Austria

[‡] Bijvoet Center for Biomolecular Research, Department of NMR Spectroscopy, Utrecht University, Padualaan 8, 3584 CH Utrecht, The Netherlands

[*] Corresponding author. E-mail: abonvin@nmr.chem.uu.nl

The simulations were done in the Bijvoet Center for Biomolecular Research, Department of NMR Spectroscopy, Utrecht University, Padualaan 8, 3584 CH Utrecht, The Netherlands

Abstract

The glucocorticoid receptor (GR) is a hormone dependent nuclear receptor that regulates gene transcription when bound to the glucocorticoid response element (GRE). The GRE acts as an allosteric effector, inducing a structural change in the glucocorticoid receptor DNA–binding domain (GR DBD) upon binding, thereby switching the GR to an active conformation. A similar conformational change can be induced by two single point mutations: *Ser459Ala* and *Pro493Arg*. Structural and dynamical aspects of the conformational switch have been investigated by molecular dynamics simulations. Our results indicate that these two mutants, which share a similar phenotype, exert their action at a structural level through different mechanisms. In the Arg^{493} mutant, the D–loop and the second helix are stabilized in a conformation that preforms the protein–protein dimer interface. In the Ala^{459} mutant, the structurally important hydrogen bond between Arg^{496} and Ser^{459} is missing, which leads to a core reorganization and a reorientation of the second helical region. Although remote, both in sequence and three dimensional structure, these two mutations induce structural changes that are ultimately reflected in similar regions of the GR DBD structure, namely the D–loop and the short second helical region. These correspond to hot area of the GR DBD that are important both for DNA–binding and for the proper formation of the protein–protein interface. The conformational rearrangements in these area are proposed to decrease unfavorable protein–DNA and protein–protein contacts and allow unspecific DNA–binding leading to

the squelching phenotype of the mutants. The GR DBD can thus exist in two states, a transcriptionally active and an inactive state. Switching between these states can be accomplished either by GRE binding or by the described mutations.

Keywords: Glucocorticoid receptor, mutations, specific and unspecific DNA binding, molecular dynamics, GROMOS96. [1]

Introduction

The superfamily of nuclear receptors is a class of transcription factors that are directly activated by the binding of hydrophobic signaling molecules, such as lipophilic hormones.[1–3] These hormones, including steroids, retinoids, tyroid hormones and vitamin–D_3 are potent regulators of cell differentiation and of organ physiology and development.

The glucocorticoid receptor (GR) is a steroid hormone receptor that regulates the transcriptional activity of linked promoters.[1,4] GR consists of a variable terminal A/B region (the transactivation domain), a C region corresponding to the conserved DNA–binding domain (DBD), an invariable hinge region D, a conservative ligand binding domain (LBD) E and a variable F–region.

[1]Abbreviations used: GR, glucocorticoid receptor; DBD, DNA binding domain; GR DBD, glucocorticoid receptor DNA binding domain; LDB, ligand binding domain; GRE, glucocorticoid response elements; MD, molecular dynamics; NMR, nuclear magnetic resonance; WT, wild type GR structure solved by NMR; XW, wild type GR structure solved by Xray crystallography; SA, alanine mutant GR structure solved by NMR; PR, arginine mutant GR structure solved by NMR; NR, hybride arginine mutant GR structure based on NW; XR, hybride arginine mutant GR structure based on XW; NA, hybride alanine mutant GR structure based on NW; XA, hybride alanine mutant GR structure based on XW; SPC, single point charge water model; ASA, accessible surface area

Domain E converts the receptor to a transcriptionally active state upon hormone binding. The active GR binds *in vivo* as a dimer specifically to the glucocorticoid response elements (GRE).[5–7] The GRE is composed of a highly conserved, but imperfect palindromic DNA sequence. The two binding sites consist each of six base pairs separated by 3 spacer nucleotides.[8,9] The right half–site is highly conserved, whereas the left site shows more variability.

The GR DBD contains two zinc finger motifs in which each zinc atom is coordinated by four cysteines (Figure 1a). The structure of the free GR DBD in solution has been determined by NMR spectroscopy[10–13] and the DNA–bound complex by X–ray crystallography.[14]

Binding of the GR to the GRE induces two notable conformational changes in the GR DBD: the D–loop reorients, which creates the dimer interface allowing contacts with its opposite monomer. Secondly, the distorted second helix is stabilized by establishing both DNA and dimer contacts.[11,12,14] The fact that the formation of the protein–protein dimer interface occurs only after DNA–binding is supported by the observation that the GR DBD is monomeric in solution but dimerizes cooperatively upon binding to the GREs.[5,10,14,15] Mutations in the dimer interface lead to a loss of cooperative DNA–binding, resulting in the loss of transcriptional activity.[16,17] In the crystal structure of GR DBD the dimer interface is located on top of the minor groove and involves the D–loop and the second helix region (Figure 1c). In the D–loop, Ala^{477} and Ile^{483} make hydrophobic contacts and a salt bridge is formed between Arg^{479} and Asp^{481}. The second helix is oriented towards the minor groove with the positively charged side chains Arg^{486}, Arg^{489} and

Lys^{490} making salt bridges with the DNA backbone.

Two single point mutations, *Ser459Ala* in the recognition helix and *Pro493Arg* at the beginning of the third helix, are particularly interesting (Figure 1a). Both mutation sites are located at the DNA–binding interface. These mutations manifest the same phenotype[13,18] when expressed in yeast. Both mutations result in a hormone dependent growth defect, which is in contrast to the wild type receptor. This growth defect is probably due to interference with the normal transcription of yeast genes.[19] Under low copy conditions the wild type and mutant receptors are indistinguishable in enhancing the transcription of reporter genes. Under high copy conditions, however, the mutants are less active. It is likely that this effect originates from squelching: the receptor can interact, without requiring specific binding to GRE, with one or more transcription factors needed for normal transcription, thereby reducing the transcription controlled by the yeast promoters by limiting their availability.[20] The mutant receptors are thus able to bind target factors in circumstances in which the wild type receptor does not. It has been suggested[13] that these mutations mimic the allosteric effect of the DNA. The NMR solution structures of the two mutants[13] have revealed folds similar to the one found in the DNA–bound crystal structure (Figure 1b). The mutations lead therefore to conformational changes that mimic the active, DNA–bound conformation in solution, thereby activating signaling without requiring the allosteric effect of binding to the GRE.

Here we present the results of extensive molecular dynamics (MD) simulations of wild type and single mutants (*Pro493Arg* and *Ser459Ala*) of the

GR DNA–binding domain. This work was initiated in order to obtain better insight into the conformational changes induced by the two single point mutations and a better understanding of how these mutations can mimic the allosteric effect produced by DNA–binding by inducing conformational changes at remote locations (up to 2 nm) while affecting the local structure only in a minor way. For this, we will compare MD simulations of wild type and mutant GR DBD structures, starting both from free and DNA–bound conformations. We will show that the *Pro493Arg* mutation results in a DNA–bound conformation in which the short second helix is stabilized by a hydrogen–bonding network involving Arg^{489}. As a result, the dimer interface involving Ile^{487} among others is preformed and the protein is switched to an active conformation. In the wild type simulations, this helix is unstable and disappears. In the *Ser459Ala* mutant a higher mobility of the core of the protein is observed due to a missing structurally important hydrogen bond to Arg^{496}. The changes in the core of the GR DBD are propagated to the short second helix region modifying its three dimensional orientation and position. This modulation of the binding interface geometry changes the DNA–binding ability of this mutant. Finally, the implications for DNA–binding will be discussed.

Results and Discussion

The Starting Structures

The experimental GR DBD structures give a static picture of the different conformations arising from the allosteric effect due to DNA–binding or induced by the two mutations described above. These structures, determined by NMR spectroscopy[13] and X-ray crystallography,[14] served as the four basic starting structures for this project (Figure 1b). Three monomeric NMR solution structures[13] were used: the wild type (NW) GR DBD sequence, the *Ser459Ala* (SA) and the *Pro493Arg* (PR) mutants, respectively. The X-ray structure[14] (XW) corresponds to one protein monomer from the homodimer DNA–complex. The four experimentally solved structures are rather similar (pairwise backbone rmsd values between 0.07 and 0.19 *nm*) with XW, PR and SA showing the same fold. The major differences between all structures are located in the D–loop, with additional minor differences in the second helix region. In the solution wild type structure (NW) the D–loop is rotated by about 90° with respect to the DNA–bound wild type structure (XW) whereas in both mutants (SA and PR) it adopts a similar orientation as in the DNA–bound wild type structure (XW) (Figure 1b). The short second helix is present in the DNA–bound structure (XW). In solution, however, no clear picture of its conformation can be deduced from the various NMR studies: it is present in some structures,[12,13] but missing in others.[10,11]
Several NMR relaxation studies on the GR have been published.[13,21–23] They all agree in showing no significant enhanced mobility in the nano– to picoseconds time range. In the case of the estrogen receptor DBD, motions in the micro to millisecond time scale have been monitored in the D–loop and the second helix region[23] indicative of slow conformational exchange. In con-

trast, in the same work, much less flexibility was found for GR DBD. Only the region between the D–loop and the second helix displayed contribution from conformational exchange while no significant mobility was monitored in the D–loop and the second helix regions themselves. This conformational exchange was interpreted in terms of intramolecular rather than intermolecular events supporting the picture, that the GR DBD exists as monomer in solution.[23]

In order to sample the phase space of the GR DBD as completely as possible and to characterize the structural and dynamical phenomena associated with the single point mutants, simulations were carried out, starting from the four experimentally solved structures and additional starting structures were generated from the experimentally solved wild type structure by mutating either Ser^{459} to Ala^{459} or Pro^{493} to Arg^{493}. A total of 8 simulations were run for 10 ns in explicit water under periodic boundary conditions in neutralized systems using the GROMOS 43A1 force field[24] (see Material and Methods). An overview of the 8 systems is given in Table 1, together with the corresponding abbreviations we will be using in the following.

Stability of the Simulations

The stability of the various simulations was monitored by following a number of quantities such as positional backbone root mean square deviations (rmsd) from the starting structures, radius of gyration, number of hydrogen bonds, accessible surface area, various energy terms and the sec-

ondary structure elements. All simulations showed stable trajectories and the various parameters reached a plateau after a few nanoseconds (Table 2). As a representative example, the secondary structure elements of the NW, PR and SA simulations are shown in Figure 2: the main secondary structure elements are conserved throughout the simulation. Most of the differences are observed in the β–hairpin (residues Gly^{449} – Tyr^{456}) and in the second helix (residues Ile^{487}-Asn^{491}). The latter will be discussed in detail below.

Arginine Mutant

The structural differences between the starting structures (PR, XR, and NR) of the three *Pro493Arg* mutant simulation are most pronounced in the D–loop region as already discussed above. Two of these simulations start with the D–loop in an active DNA–bound conformation (PR and XR), in contrast to the third simulation (NR) that starts from the free wild type solution structure (Figure 1b). In the latter simulation a transition can be seen after approximately 6 ns: the D–loop begins to rotate and converges within 0.2 nm from the DNA–bound conformation. The conformation of the D–loop of all *Pro493Arg* mutant simulations (PR, XR, and NR) converges to a fold analogous to that found in the DNA–bound complex. A comparison of the D–loop conformation of these three simulations and of the NW simulation is shown as a pairwise rmsd matrix in Figure 3. The presence of the amide proton in the arginine mutant allows the formation of a hydrogen bond between the Arg^{493} amide proton and the carbonyl oxygen of Leu^{475}.

This additional hydrogen bond could explain the observation that all arginine mutant simulations are converging to the same fold while neither the alanine nor the wild type simulations converge. In the later simulations a proline is found at position 493 and this proline can not form the hydrogen bond to Leu^{475}.

A second region of the GR DBD structure appears to be important for function: the second helix region (Ile^{487}–Asn^{491}) located at the dimer and DNA–binding interface. The conformation of this region is clearly influenced by this mutation. A consistent picture of the role of the arginine mutant emerged from all our *Pro493Arg* mutant simulations: the short second helix is stabilized by the presence of Arg^{493}. Irrespective of the starting conformation (arginine mutant structure (PR), DNA–bound structure (XR), or wild type "free" solution structure (NR)) the helix appears in the early stage of the simulation and it's fold is close to the experimentally solved DNA–bound GR DBD structure (Figure 4c). In contrast, in the wild type simulation (NW), the second helix region remains in its "free" conformation that would protrude into the DNA if no conformational changes were to take place upon DNA–binding (Figure 4b). The hydrogen bonding pattern in the second helix region seems to be the switch for the conformational transition (Table 3). The peptidic bond between Arg^{488} and Arg^{489} plays thereby a central role. The α–helical hydrogen bonds are broken by the flip of this peptidic bond. In this way, the central α–helical hydrogen bond between the carbonyl oxygen of Arg^{489} and the amide proton of Cys^{492} and the N–cap stabilizing hydrogen bond between the amide proton of Arg^{489} and the carbonyl oxygen

of Asp^{485} can no longer exist and the helix disappears. Two new hydrogen bonds between the amide proton of Asp^{485} and the carbonyl oxygen of Arg^{488} and between the amide proton of Arg^{489} and the carbonyl oxygen of Ile^{487} are formed, stabilizing the bend structure. The rotation of the peptidic bond between Arg^{488} and Arg^{489} can thus trigger the folding and unfolding of the α–helix, switching between a bend and a helical conformation. The formation of the bend is observed in all simulations where the helical structure element disappears. In contrast, in the wild type protein, as we will discuss below, it is the hydrogen bonding of Arg^{496} to the DNA that triggers the conformational change.

A comparison of this short second helix region between the arginine mutant simulations (PR, XR, and NR), and the wild type simulations (XW, and NW) clearly reveals the importance of this specific conformation: in the second helix region of the *Pro493Arg* mutant simulations the residues and their side chains are positioned in a highly specific manner, similar to the experimentally solved GR DBD structures in the DNA complex. The backbone conformation plays thus an important role in modulating its side chain orientations leading to the formation of the DNA–bound conformation. In particular, when the helix is formed, the hydrophobic amino acid Ile^{487} is positioned in an orientation that preforms the dimer interface (Figure 4c). This residue is involved in inter–monomer hydrophobic interactions in the DNA–bound complex (Figure 4a). In the wild type simulations this side chain adopts a different orientation that does not allow the formation of these hydrophobic contacts.

Alanine Mutant

Although both mutants share a similar squelching phenotype, the structural changes induced by the *Ser459Ala* mutant differ from those identified in the arginine mutant. The key element in the changes induced by the alanine mutation is the missing hydrogen bond between the side chains of Arg^{496} and the mutated serine at position 459. This hydrogen bond is present in all wild type and arginine mutant simulations. In contrast, in the alanine mutant, the side chain of Arg^{496} has a larger conformational freedom. Due to this missing hydrogen bond, the core helices (the recognition helix and the third helix) reorient slightly, their N–caps moving closer to each other. This is observed in both the SA and XA simulations. An essential dynamics analysis[25,26] clearly reveals this rearrangement (Figure 5). No such rearrangement can be identified in the wild type or arginine–mutant simulations. The movement of the third helix towards the recognition helix causes a change in the position and orientation of the second helix region (Ile^{487} to Asn^{491}) relative to the recognition helix (Gly^{458} to Glu^{469}). Because of that, the global orientation of the second helix region in the alanine mutant differs from the wild type structure. In particular, the amino acid side chains in this region adopt different orientations compared to the wild type that will no longer protrude into the DNA upon binding. For example, in the wild type, the side chain of Ile^{487} is oriented towards the DNA–backbone, whereas in the alanine mutant this side chain reorients towards the opposite direction (Figure 4d). The

change in the orientation of the second helix region thus reduces unfavorable contacts between the GR DBD and the DNA that would be present in the first step of binding by the wild type GR DBD.

The alanine mutation also induces changes in the D–loop region. No convergence in this region could however be reached between the various systems within the time scale of our simulations. The two *Ser459Ala* mutant simulations (SA and XA) starting with a fold similar to the DNA–bound conformation remain close to it (within 0.2 nm). In the alanine mutant simulation starting from the inactive free conformation (NA), a rotation of the D–loop towards the active conformation is observed, but this conformational transition does not yet converges to the fold of the other two alanine simulations. The time window of our simulations is too short for sampling the complete transition. Nevertheless, this behavior suggests that the active D–loop conformation is most probably the more stable conformation. The removal of the structurally important hydrogen bond between Arg^{496} and Ser^{459} affects thus the conformation of the D–loop and second helix region. Interestingly, in the DNA–complex, this hydrogen bond is disrupted and, instead, Arg^{496} is hydrogen bonded to the DNA. Our results indicate that Arg^{496} could be the switch that modulates the conformation of the wild type GR DBD. This will be discussed in the next section.

Significance for DNA–binding

The mutants, *Ser459Ala* and *Pro493Arg*, although remote both in se-

quence and structure, induce conformational changes in a similar region of the GR DBD, namely the D–loop and the second helix region. These two structural elements are implicated in both protein-protein interactions upon dimerization and minor groove DNA–binding. The two mutants exert their effect by different mechanisms. The *Pro493Arg* mutant provides additional hydrogen bonding capabilities that lead to a stabilization of the second helix and of the DNA–bound conformation of the D–loop. In contrast, in the *Ser459Ala* mutant, the structurally important hydrogen bond between the guanido group of Arg^{496} and the hydroxyl of Ser^{459} is lacking. This allows a slight rearrangement of the core helices that is ultimately propagated to the second helix region (Figure 5). This mechanism of action is particularly interesting in the light of the binding of the GR DBD to DNA. The same Arg^{496} in the protein–DNA complex is indeed no longer hydrogen–bonded to the Ser^{459} but to the DNA bases in the major groove at the sequence–specific recognition site. In the MD simulation starting from the wild type DNA–bound conformation (XW), the arginine side–chain moves back toward the core of the GR DBD and the hydrogen bond to Ser^{459} is recovered after 4 *ns*. Once formed, it is stable for the remaining of the simulation. This process can be interpreted as the first, reverse step of the binding of the GR DBD to its specific DNA operator. Based on this, we propose a model of how the DNA exerts its allosteric effect onto the GR DBD. Upon specific DNA–binding, the Arg^{496} side–chain is pulled out toward the DNA, thereby breaking the hydrogen bond to Ser^{459}. This allows a slight rearrangement of the core helices (helices I and III) that is propagated to the D–loop and second helix region.

The modulation of the orientation of the side–chains in these regions preforms the dimer interface and leads to favorable interactions with the DNA in the minor groove. The second GR DBD unit can then bind, resulting in dimerization and activation (Figure 6 upper panel). This mechanism is in line with the mechanism proposed by Yamamoto et al.[18] and the observed cooperativity of the binding.[6] Only specific DNA–binding will provide the necessary energy to break the Arg^{496}–Ser^{459} hydrogen bond and induce the conformational changes in the GR DBD. In the case of the two single point mutants, however, no high energetic price needs to be paid since the D–loop and the second helix region are already preorganized for DNA–binding and protein dimerization. Because of that, any unspecific DNA–binding event will lead to dimerization and activation (Figure 6 lower panel). This can explain the squelching phenotype of these two mutants: already upon unspecific DNA–binding will the GR be activated and recruit the necessary transcription factors, thereby decreasing their availability for normal gene expression. This effect will be more dramatic when GR is overexpressed: the GR mutants present at higher concentrations under such conditions will lower the availability of those transcription factors.

Conclusions

Both single point mutations (*Ser459Ala* and *Pro493Arg*) modulate the structure of the GR DBD and have been shown to alter the normal gene expression by squelching.[13,18] Although these mutations are remote, both in sequence and three dimensional structure, they induce structural changes

that are ultimately reflected on a similar region of the GR DBD structure, namely in the DNA–binding and dimerization interface. Our MD simulations of wild type and mutant sequences have revealed distinct structural transitions depending on the sequence. By its additional hydrogen bonding capacities, the arginine mutant stabilizes the D–loop and the short second α–helix in a conformation similar to the conformation in the DNA–bound complex. This preforms the DNA–binding and protein dimerization interfaces already in the free form. The modulation of the structure by the alanine mutation has a different origin with, as key element, the disruption of the structurally important hydrogen bond between Arg^{496} and Ser^{459}. It is remarkable that both mutants, which share a similar phenotype, exert their action at a structural level through quite different mechanisms.

Based on our results for the alanine mutant, we have proposed a model for the allosteric action of the DNA operator onto the GR DBD: the breaking of the hydrogen bond between Arg^{496} and Ser^{459} induced by binding of the wild type GR to DNA allows a slight core rearrangement that leads to changes in the D–loop and the second helix regions, enabling dimerization of the GR. Only specific DNA–binding will provide sufficient energy to induce those changes. In the case of the mutants, which already have favorable conformations for DNA–binding and dimerization, the energetic price to pay is lower and any unspecific DNA–binding event will lead to activation. As a consequence of this unspecific activation, transcription factors will be recruited, decreasing their availability for normal gene expression and causing the squelching phenomenon. Our results support the notion that the GR

DBD can exist in two conformational states, a transcriptionally active and an inactive state. Switching between these states can be accomplished either by GRE binding or by mutating Ser^{459} into an alanine or Pro^{493} into an arginine.

Material and Methods

Starting Structures

Eight MD simulations of the GR DBD and its variants were carried out. From the wild type crystal structure of the GR DNA complex (PDB entry 1GLU)[14] the GR DBD molecule with the best stereochemical parameters (secondary structure, Ramachandran–plot, g–factor, number of hydrogen bonds as evaluated with Procheck[27] and MolMol[28]) was selected (the unit cell contained two GR DBD molecules). Three NMR solution structures[13] were available corresponding to the wild type sequence and the two point mutations *Ser459Ala* and *Pro493Arg*. From each NMR ensemble, one representative structure was selected, applying the same stereochemical criteria as used for the DNA–bound GR DBD crystal structure. From these four experimentally solved structures four additional starting conformations were generated by introducing the simple point mutations into the free and DNA–bound wild type structures. A total of 8 simulations was thus performed: two with the wild type sequence (XW, NW), three with the *Pro493Arg* mutation (PR, XR, and NR) and three with the *Ser459Ala* mutation (SA, XA,

and NA). These are summarized in Table 1. The *in silico* mutations were introduced using the program Setor.[29] The side chain of the mutated residues were rotated if needed to avoid sterical clashes.

System Setup and Equilibration

The GROMOS96 molecular dynamics package[24,30] was used with the GROMOS 43A1 force field.[31] The parameters for the two zinc ions in the GR DBD were taken from the literature.[32] The force constants were chosen such as to ensure stable trajectories and to be in line with the GROMOS 43A1 force field parameters. These parameters are listed in Table 4. The starting protein structures were first energy minimized by steepest descent energy minimization. Then, the GR DBD was solvated in a truncated octahedron water box with a minimum solute–wall distance of 1.4 nm using the single point charge (SPC) water model.[33] Periodic boundary conditions were applied. The protein coordinates were kept fixed for the first 500 steps of steepest descent energy minimization. The system was then electro-neutralized by replacing the water molecules with the highest electrostatic potential energy with Cl^- ions and again submitted to 500 steps of steepest descent energy minimization. This was followed by a 100 ps equilibration period during which position restraints[34,35] were applied on the GR DBD with decreasing force constants of 5000, 500, 50, 5, 0 $kJ\,mol^{-1}\,nm^{-2}$ for each 20 ps period, respectively. The system was then set completely free and the production run started for a total period of 10 ns.

Molecular Dynamics Simulations

The simulations were run for a time period of 10 *ns* at 300 *K*. Solute, solvent and counterions were independently weakly coupled to a reference temperature bath[36] with a coupling constant τ of 0.1 *ps*. The initial velocities were taken from a Maxwellian distribution at the chosen temperature. The pressure was maintained by weakly coupling the system to an external pressure bath at one atmosphere with a coupling constant of 0.5 *ps*. All bonds were constrained using SHAKE[34,35] with a relative tolerance of $1.0*10^{-4}$. The cutoff for electrostatic and van der Waals interactions was set to 1.4 *nm*. The long range electrostatic interactions beyond the 1.4 *nm* cutoff were treated with the generalized reaction field model[37] using a dielectric constant of 54.[33] Non–bonded interactions were calculated using twin range cutoffs[38] of 0.8 and 1.4 *nm*. The non-bonded pair list was updated every 5 steps using the extended cutoff implementation:[39] an extended pair list generated with a 1.8 *nm* cutoff was used to update the normal non–bonded pair list. The extended pair list itself was automatically updated once an atom moved by more than 0.4 *nm* (extended cutoff–long range cutoff), typically every 50 to 100 steps. Energies and coordinates were saved every 250 step. A time step of 2 *fs* was used for the integration.

Acknowledgments

T.S. and H.S. acknowledge the financial support from the "Fond zur Förderung der wissenschaftlichen Forschung", FWF Project Nr. P13909-CHE.

References

1. Beato, M., Herrlich, P. & Schutz, G. (1995). Steroid hormone receptors: many actors in search of a plot. *Cell* **83** (6), 851–7.

2. Mangelsdorf, D. J., Thummel, C., Beato, M., Herrlich, P., Schutz, G., Umesono, K., Blumberg, B., Kastner, P., Mark, M., Chambon, P. & Evans, R. M. (1995). The nuclear receptor superfamily: the second decade. *Cell* **83** (6), 835–9.

3. Collingwood, T. N., Urnov, F. D. & Wolffe, A. P. (1999). Nuclear receptors: coactivators, corepressors and chromatin remodeling in the control of transcription. *J. Mol. Endocrinol.* **23** (3), 255–75.

4. Tsai, M. J. & O'Malley, B. W. (1994). Molecular mechanisms of action of steroid/thyroid receptor superfamily members. *Annu. Rev. Biochem.* **63**, 451–86.

5. Härd, T., Dahlman, K., Carlstedt-Duke, J., Gustafsson, J. A. & Rigler, R. (1990). Cooperativity and specificity in the interactions between dna and the glucocorticoid receptor dna-binding domain. *Biochemistry* **29** (22), 5358–64.

6. Zilliacus, J., Wright, A. P., Carlstedt-Duke, J. & Gustafsson, J. A. (1995). Structural determinants of dna-binding specificity by steroid receptors. *Mol. Endocrinol.* **9** (4), 389–400.

7. Starr, D. B., Matsui, W., Thomas, J. R. & Yamamoto, K. R. (1996). Intracellular receptors use a common mechanism to interpret signaling information at response elements. *Genes Dev.* **10** (10), 1271–83.

8. Beato, M., Chalepakis, G., Schauer, M. & Slater, E. P. (1989). Dna regulatory elements for steroid hormones. *J. Steroid Biochem.* **32** (5), 737–47.

9. Beato, M. (1989). Gene regulation by steroid hormones. *Cell* **56** (3), 335–44.

10. Härd, T., Kellenbach, E., Boelens, R., Maler, B. A., Dahlman, K., Freedman, L. P., Carlstedt-Duke, J., Yamamoto, K. R., Gustafsson, J. A. & Kaptein, R. (1990). Solution structure of the glucocorticoid receptor dna-binding domain. *Science* **249**, 157–60.

11. van Tilborg, M. A., Bonvin, A. M., Härd, K., Davis, A. L., Maler, B., Boelens, R., Yamamoto, K. R. & Kaptein, R. (1995). Structure refinement of the glucocorticoid receptor-dna binding domain from nmr data by relaxation matrix calculations. *J. Mol. Biol.* **247** (4), 689–700, doi:10.1006/jmbi.1995.0173.

12. Baumann, H., Paulsen, K., Kovaćs, H., Berglund, H., Wright, A. P., Gustafsson, J. A. & Härd, T. (1993). Refined solution structure of the glucocorticoid receptor dna-binding domain. *Biochemistry* **32** (49), 13463–71.

13. van Tilborg, M. A., Lefstin, J. A., Kruiskamp, M., Teuben, J., Boelens, R., Yamamoto, K. R. & Kaptein, R. (2000). Mutations in the glucocorticoid receptor dna-binding domain mimic an allosteric effect of dna. *J. Mol. Biol.* **301** (4), 947–58, doi:10.1006/jmbi.2000.4001.

14. Luisi, B. F., Xu, W. X., Otwinowski, Z., Freedman, L. P., Yamamoto, K. R. & Sigler, P. B. (1991). Crystallographic analysis of the interaction of the glucocorticoid receptor with dna [see comments]. *Nature* **352**, 497–505. Comment in: Nature 1991 Aug 8;352(6335):478-9.

15. Lefstin, J. A. & Yamamoto, K. R. (1998). Allosteric effects of dna on transcriptional regulators. *Nature* **392**, 885–8, doi:10.1038/31860.

16. Yamamoto, K. R., Pearce, K., Thomas, J. & Miner, J. N. (1992). *Transcriptional Regulation* pp. 1169–1170. New York: Cold Spring Harbor Laboratory Press.

17. Heck, S., Kullmann, M., Gast, A., Ponta, H., Rahmsdorf, H. J., Herrlich, P. & Cato, A. C. (1994). A distinct modulating domain in glucocorticoid receptor monomers in the repression of activity of the transcription factor ap-1. *EMBO J.*, **13** (17), 4087–95.

18. Lefstin, J. A., Thomas, J. R. & Yamamoto, K. R. (1994). Influence of a steroid receptor dna-binding domain on transcriptional regulatory functions. *Genes Dev.*, **8**, 2842–56.

19. Godowski, P. J., Picard, D. & Yamamoto, K. R. (1988). Signal

transduction and transcriptional regulation by glucocorticoid receptor-lexa fusion proteins. *Science*, **241**, 812–6.

20. Gill, G. & Ptashne, M. (1988). Negative effect of the transcriptional activator gal4. *Nature*, **334**, 721–724.

21. Berglund, H., Kovaćs, H., Dahlman-Wright, K., Gustafsson, J. A. & Härd, T. (1992). Backbone dynamics of the glucocorticoid receptor dna-binding domain [published erratum appears in biochemistry 1993 apr 13;32(14):3829]. *Biochemistry*, **31** (48), 12001–11.

22. Eriksson, M. A., Berglund, H., Härd, T. & Nilsson, L. (1993). A comparison of 15n nmr relaxation measurements with a molecular dynamics simulation: backbone dynamics of the glucocorticoid receptor dna-binding domain. *Proteins*, **17** (4), 375–90.

23. Wikström, A., Berglund, H., Hambraeus, C., van den Berg, S. & Härd, T. (1999). Conformational dynamics and molecular recognition: backbone dynamics of the estrogen receptor dna-binding domain. *J. Mol. Biol.*, **289** (4), 963–79, doi:10.1006/jmbi.1999.2806.

24. van Gunsteren, W., Daura, X. & Mark, A. (1998). Gromos force field. *Ency. Comp. Chem.*, **2**, 1211–1216, doi:10.1002/0470845015.cga011.

25. Amadei, A., Linssen, A. B. & Berendsen, H. J. (1993). Essential dynamics of proteins. *Proteins*, **17** (4), 412–25.

26. de Groot, B. L., Hayward, S., van Aalten, D. M., Amadei, A. & Berendsen, H. J. (1998). Domain motions in bacteriophage t4 lysozyme: a comparison between molecular dynamics and crystallographic data. *Proteins*, **31** (2), 116–27, doi:10.1002/(SICI)1097-0134(19980501)31:2<116::AID-PROT2>3.0.CO;2-K.

27. Morris, A. L., MacArthur, M. W., Hutchinson, E. G. & Thornton, J. M. (1992). Stereochemical quality of protein structure coordinates. *Proteins*, **12** (4), 345–64.

28. Koradi, R., Billeter, M. & Wüthrich, K. (1996). Molmol: a program for display and analysis of macromolecular structures. *J. Mol. Graph.*, **14** (1), 51–5, 29–32.

29. Evans, S. V. (1993). Setor: hardware-lighted three-dimensional solid model representations of macromolecules. *J. Mol. Graph.*, **11** (2), 134–8, 127–8, doi:10.1016/0263-7855(93)87009-T.

30. Scott, W., Hünenberger, P., Tironi, I., Mark, A., Billeter, S., Fennen, J., Torda, A., Huber, T., Krüger, P. & van Gunsteren, W. (1999). The gromos biomolecular simulation program package. *J. Phys. Chem. A*, **103**, 3596–3607, doi:10.1021/jp984217f.

31. Daura, X., Mark, A. & van Gunsteren, W. (1998). Parametrization of aliphatic chn united atoms of gromos96 force field. *J. Comput. Chem.*, **19**, 535–547, doi:10.1002/(SICI)1096-987X(19980415)19:5<535::AID-JCC6>3.0.CO;2-N.

32. Eriksson, M. A., Härd, T. & Nilsson, L. (1995). Molecular dynamics simulations of the glucocorticoid receptor dna-binding domain in complex with dna and free in solution. *Biophys. J.*, **68** (2), 402–26.

33. Berendsen, H. C., Postma, J. P. M., van Gunsteren, W. F. & Hermans, J. (1981). *Intermolecular Forces*, chapter Interaction Models for Water in Relation to Protein Hydration, pp. 331–342. Dordrecht: Reidel.

34. van Gunsteren, W. F. & Karplus, M. (1982). Effect of constraints on the dynamics of macromolecules. *Macromolecules*, **15**, 1528–1544.

35. Ryckaert, J. P., Ciccotti, G. & Berendsen, H. J. C. (1977). Numerical integration of the cartesian equations of motion of a system with constraints: molecular dynamics of n-alkanes. *J. Comput. Phys.*, **23**, 327–341.

36. Berendsen, H. J. C., Postma, J. P. M., van Gunsteren, W. F., DiNola, A. & Haak, J. R. (1984). Molecular dynamics with coupling to an external bath. *J. Chem. Phys.*, **81**, 3684–3690, doi:10.1063/1.448118.

37. Tironi, I. G., Sperb, R., Smith, P. E. & van Gunsteren, W. F. (1995). A generalized reaction field method for molecular dynamics simulations. *J. Chem. Phys.*, **102**, 5451–5459, doi:10.1063/1.469273.

38. van Gunsteren, W. F. & Berendsen, J. C. (1990). Computer simulation of molecular dynamics: methodology, applications, and perspectives in chemistry. *Angew. Chem. Int. Ed. Engl.*, **29**, 992–1023.

39. Bonvin, A. M. J. J., Mark, A. E. & van Gunsteren, W. F. (2000). The gromos96 benchmarks for molecular simulation. *Comput. Phys. Commun.*, **128**, 550–557.

40. Kraulis, P. J. (1991). Molscript: a program to produce both detailed and schematic plots of protein structures. *J. Appl. Cryst.*, **24**, 946–950, doi:10.1107/S0021889891004399.

41. Merritt, E. A. & Bacon, D. J. (1997). Raster3d: photorealistic molecular graphics. *Meth. Enzymol.*, **277**, 505–524.

42. Martin, A. C. R. (1992). *ProFit*. SciTech Software.

43. Berendsen, H. J. C., van der Spoel, D. & van Drunen, R. (1995). Gromacs: a message-passing parallel molecular dynamics implementation. *Comp. Phys. Comm.*, **91**, 43–56.

44. Lindahl, E., Hess, B. & van der Spoel, D. (2001). Gromacs 3.0: a package for molecular simulation and trajectory analysis. *J. Mol. Mod.*, **7**, 306–317.

Figure Legends

Figure 1

Ribbon representation of GR DBD structures. a) Structure overview. b) Overlay of the 4 experimentally solved structures fitted on the core helices I and III (Gly^{458}–Glu^{469} and Pro^{493}–Ala^{503}). The region from the D–loop (Cys^{476}–Cys^{482}) to the second helix regions (Ile^{487}–Asn^{491}) is color coded: free wild type NMR structure (magenta), DNA–bound crystal structure (blue), free *Pro493Arg* NMR structure (green) and free *Ser459Ala* NMR structure (red). c) Protein–DNA complex (PDB entry 1GLU).[14] The figures were generated with Molscript[40] and Raster3D.[41]

Figure 2

Evolution of secondary structure elements as a function of time. a) free wild type (NW), b) *Pro493Arg* mutant (PR) and c) *Ser459Ala* mutant (SA). The analysis was performed with Procheck.[27]

Figure 3

Pairwise backbone rmsd matrix for the D–loop region of the free wild type (NW) and arginine mutant simulations (NR, PR, XR). Each section represents a 10 *ns* simulation. Each colored dot represents a positional rms deviation between two conformations taken from the respective tajectories

indicated on the axes and is color coded accordingly to the scale shown on the right. The conformations are taken every 0.2 ns. The structures were fitted on the core helices I and III (Gly^{458}–Glu^{469} and Pro^{493}–Ala^{503}) and the rmsd were calculated on backbone atoms of the D–loop (Cys^{476}–Cys^{482}) using Profit.[42]

Figure 4

Detailed view of the dimerization interface of the DNA complex with snapshots taken at 8 *ns* from various MD simulations. a) Crystal structure (PDB entry 1GLU)[14] and superpositions of b) the free wild type structure (NW), c) the *Pro493Arg* mutant structure (PR) and d) the *Ser459Ala* mutant structure (SA) onto the crystal structure. The structures were fitted on the backbone of the DNA–binding regions (Gly^{458}–Glu^{469} and Asn^{491}–Arg^{496}). The two GR DBD's in the crystal structure are drawn in blue and light blue, respectively. Only the backbone of the MD structures around the second helix region (Lys^{486}–Cys^{492}) is represented (yellow).

Figure 5

Representation of the eigenmode of the *Ser459Ala* (SA) MD simulation associated with the core and second helix rearrangements. The eigenvector analysis[25,26] was based on the covariance matrix calculated from the complete MD simulation run after fitting the structures on the recognition helix

(helix I). The interpolated conformations between the two extremes for the second helix region (Ile^{487}–Asn^{491}) and third helix (Pro^{493}–Ala^{503}) are color coded from blue to red. The analysis was performed using Gromacs.[43,44]

Figure 6

Schematic model of the control mechanism of the glucocorticoid receptor (GR) activation upon specific or unspecific DNA–binding of the wild type (top panel) and the two single–point mutants *Ser459Ala* and *Pro493Arg* (bottom panel).

Table 1:

Simulation systems				
GR DBD	Number of Cl^- counterions	Number of waters	Total Number of atoms	Abbreviation
DNA–bound wild type crystal structure[14]				
wild type sequence	2	5438	17033	XW
Pro493Arg mutant	3	5432	17026	XR
Ser459Ala mutant	2	5426	16995	XA
Solution NMR wild type structure[13]				
wild type sequence	2	4204	13331	NW
Pro493Arg mutant	3	4212	13366	NR
Ser459Ala mutant	2	4205	13332	NA
Solution NMR *Pro493Arg* mutant structure[13]				
Pro493Arg mutant	3	4621	14593	PR
Solution NMR *Ser459Ala* mutant structure[13]				
Ser459Ala mutant	2	3985	12672	SA

Table 2:

Structural statistics[a]				
	NW	**PR**	**NR**	**XR**
rmsd backbone (nm)[b]	0.32±0.04	0.34±0.02	0.29±0.02	0.19±0.02
rmsd heavy atoms (nm)[b]	0.41±0.04	0.46±0.02	0.39±0.02	0.29±0.02
Number of H–bonds	40±3	43±4	43±4	45±4
Radius of gyration (nm)	1.18±0.02	1.14±0.01	1.14±0.02	1.12±0.01
ASA (nm^2)	218±2	216±2	218±2	215±2
α–helix (%)	22±1	24±2	25±2	25±2
β–sheet (%)	3±3	0±0	2±3	4±3
Turn structure (%)	5±2	5±2	5±2	7±2
Bend structure (%)	11±2	15±2	10±2	12±2
	XW	**SA**	**NA**	**XA**
rmsd backbone (nm)	0.23±0.02	0.27±0.02	0.22±0.01	0.27±0.02
rmsd heavy atoms (nm)	0.35±0.02	0.38±0.02	0.37±0.02	0.36±0.02
Number of H–bonds	41±4	41±4	40±3	38±3
Radius of gyration (nm)	1.12±0.01	1.14±0.02	1.08±0.01	1.18±0.01
ASA (nm^2)	215±2	216±2	214±2	217±2
α–helix (%)	22±1	22±1	21±1	22±1
β–sheet (%)	2±2	2±2	3±2	1±2
Turn (%)	3±2	5±2	3±2	1±1
Bend (%)	18±2	15±2	19±2	19±2

[a] The average values were calculated over the time range 4.0-10.0 ns.

[b] The rmsd were calculated on all residues after fitting on the Cα atoms of the starting structure.

Table 3:

Second helix region backbone hydrogen bonds[a]									
Donor	Acceptor	NW	XW	PR	NR	XR	SA	NA	XA
Bend conformation									
Asp^{485}	Arg^{488}	36	41	–	–	–	18	84	88
Asp^{485}	Arg^{489}	9	14	–	–	–	43	9	18
Arg^{489}	Ile^{487}	40	48	–	–	–	16	6	18
Helical conformation									
Arg^{489}	Asp^{485}	30	–	90	98	99	–	8	–
Lys^{490}	Ile^{487}	14	–	80	88	88	–	7	–
Asn^{491}	Ile^{487}	–	–	38	25	24	–	–	–
Asn^{491}	Arg^{488}	28	5	38	26	32	–	–	5
Cys^{492}	Arg^{488}	2	–	92	86	95	–	7	–
[b]Arg^{493}	Asn^{491}	–	–	26	13	38	–	–	–

[a] Average percentage over the complete simulations

[b] Only the Arg^{493} mutant structures have an amide proton.

Table 4:

Force field parameters of the zinc fingers			
Interaction Term		**Value**	**Force Constant**
Bond length r_0	SG–ZN	0.2325 (nm)	$3.015{*}10^7$ $(kJ\,nm^{-2}mol^{-1})$
Bond angle θ_0	CB–SG–ZN	116.30 $(degrees)$	$0.260{*}10^3$ $(kJ\,rad^{-2}mol^{-1})$
Bond angle θ_0	SG–ZN–SG	109.50 $(degrees)$	$0.260{*}10^3$ $(kJ\,rad^{-2}mol^{-1})$
Improper angle θ_0	SG–SG–SG–SG	70.529 $(degrees)$	0.050 $(kJ\,rad^{-2}mol^{-1})$
Charge e^-	ZN	0.96 (e^-)	
Charge e^-	SG	-0.72 (e^-)	
Charge e^-	CB	-0.02 (e^-)	

Figure 1 Stockner *et al.*

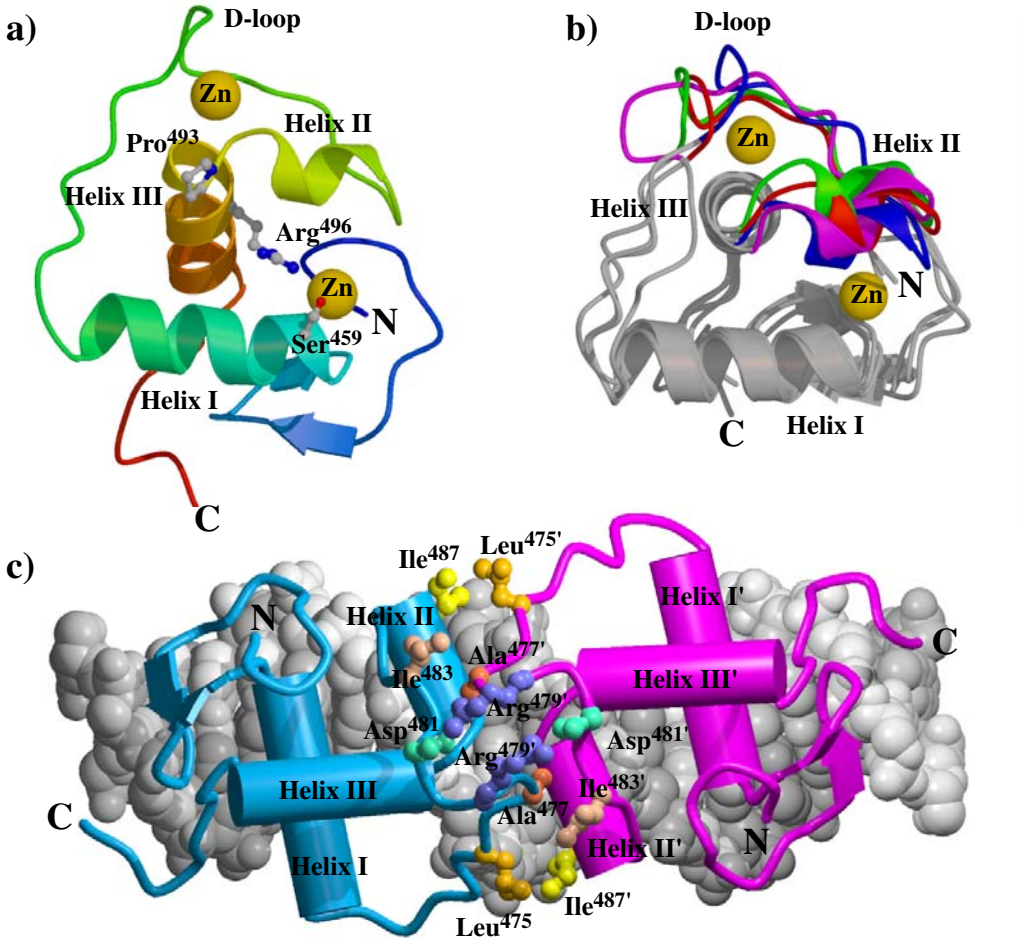

Figure 2 Stockner *et al.*

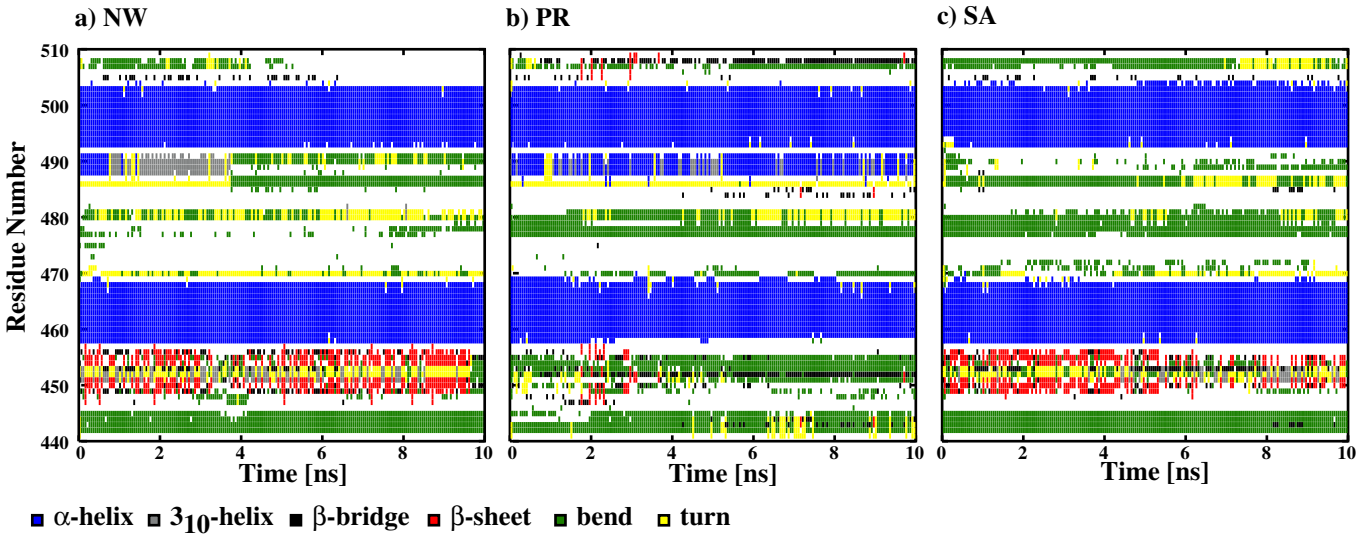

Figure 3 Stockner *et al.*

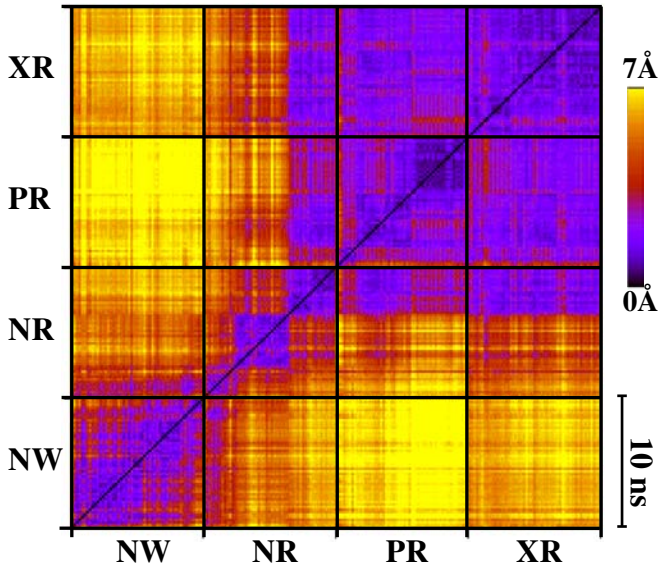

Figure 4 Stockner *et al.*

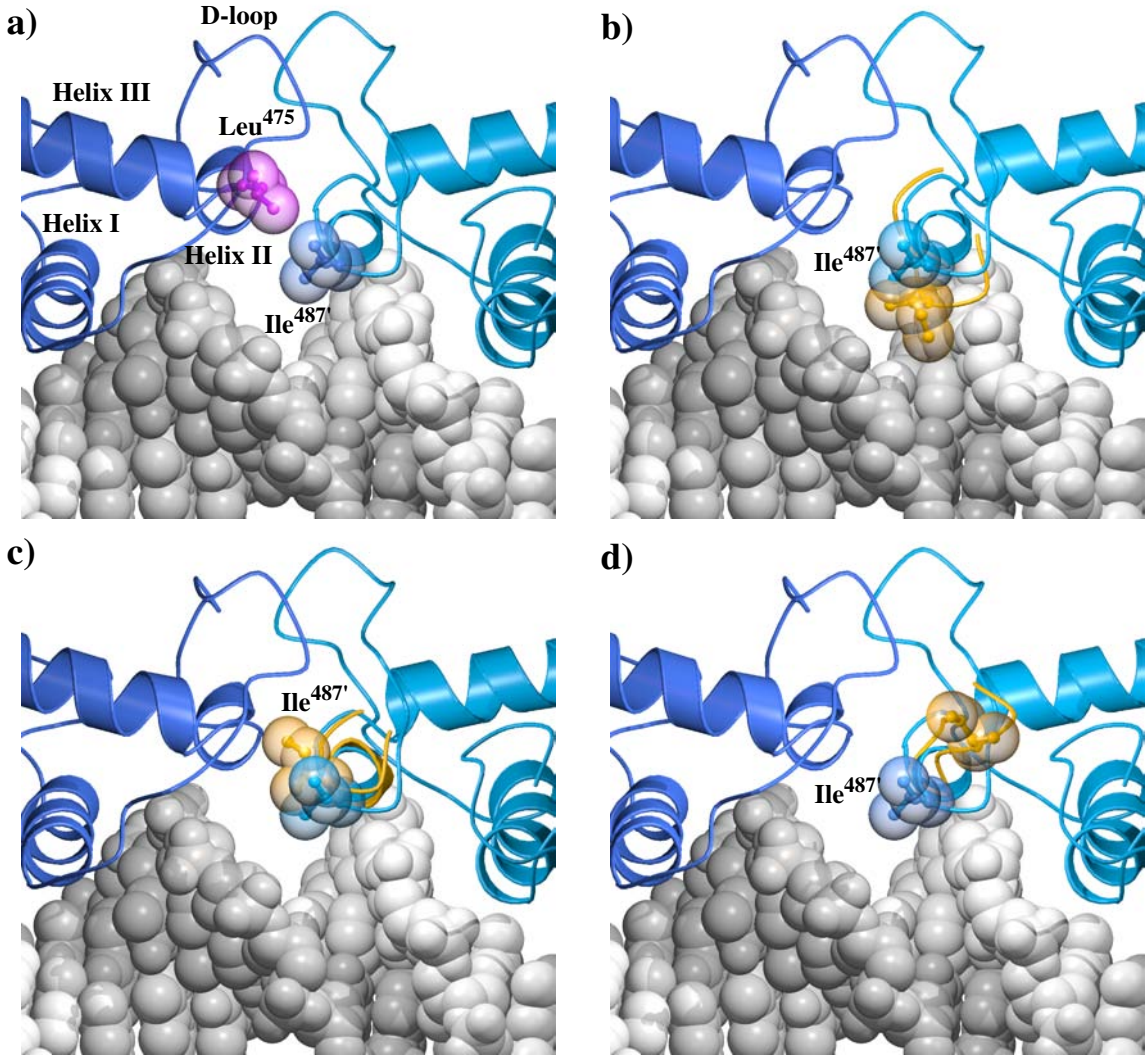

Figure 4 Stockner *et al.*

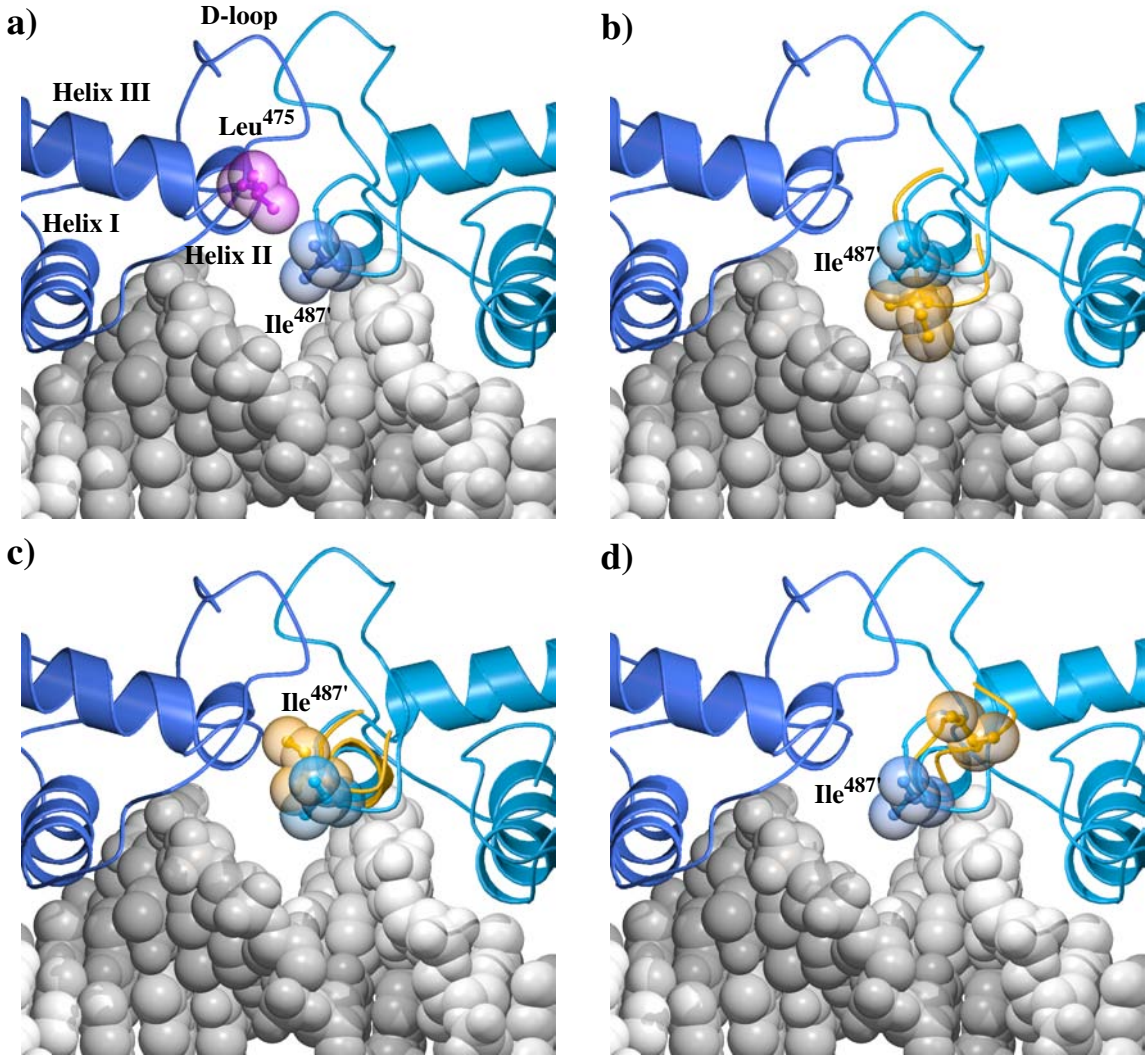

Figure 5 Stockner *et al.*

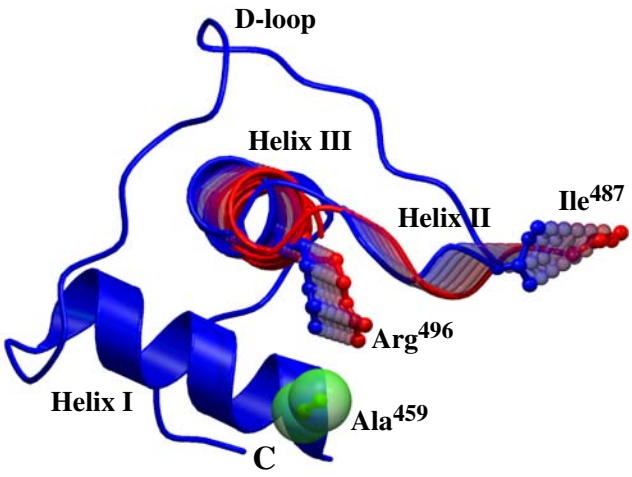

Figure 6 Stockner *et al.*